Improved Spatial Resolution in Thick, Fully-Depleted CCDs with Enhanced Red Sensitivity

Jessamyn A. Fairfield, Donald E. Groom, Stephen J. Bailey, Christopher J. Bebek, *Member, IEEE*, Stephen E. Holland, *Member, IEEE*, Armin Karcher, William F. Kolbe, Wolfgang Lorenzon, and Natalie A. Roe

***Abstract*—The point spread function (PSF) is an important measure of spatial resolution in CCDs for point-like objects, since it affects image quality and spectroscopic resolution. We present new data and theoretical developments for lateral charge diffusion in thick, fully-depleted charge-coupled devices (CCDs) developed at Lawrence Berkeley National Laboratory (LBNL). Because they can be over-depleted, the LBNL devices have no field-free region and diffusion is controlled through the application of an external bias voltage. We give results for a 3512×3512 format, 10.5 μm pixel back-illuminated p-channel CCD developed for the SuperNova/Acceleration Probe (SNAP), a proposed satellite-based experiment designed to study dark energy. The PSF was measured at substrate bias voltages between 3 V and 115 V. At a bias voltage of 115 V, we measure an rms diffusion of 3.7 ± 0.2 μm. Lateral charge diffusion in LBNL CCDs will meet the SNAP requirements.**

***Index Terms*—charge coupled device, diffusion processes, high-resistivity silicon, optical transfer functions**

I. Introduction

LATERAL charge diffusion is the drifting of carriers in the plane of the CCD as they travel from the point of generation to the potential wells where the charge is collected. Pixel size and lateral charge diffusion are the primary factors determining the spatial resolution of a CCD. In thin back-illuminated CCDs used for astronomical imaging, the lateral diffusion is approximately equal to the thickness of the field-free region, typically on the order of 5–10 μm. By contrast, the LBNL thick, fully-depleted CCDs [1] have no field-free region. Even though charge created near the backside must drift across the thick substrate (200–300 μm) to reach the pixel, the lateral diffusion can be lower than that of thin devices with sufficient over-depletion of the substrate. The thick substrate extends the detection efficiency into the near-infrared and minimizes fringing. Since lateral charge diffusion increases linearly with substrate thickness, the optimal detector is an application specific tradeoff of extended red response and PSF.

The LBNL devices are fabricated from high-resistivity (4−10 kΩ/cm), weakly doped, n-type silicon, with p-type channels made with boron implants. The charge carriers collected are holes. This design was chosen as a result of the straightforward implementation of extrinsic gettering techniques for low dark current with n-type high-resistivity silicon and for increased radiation hardness [2]. The substrate can be fully depleted with a bias voltage, typically in the range of 15–30V for a 200 μm thick CCD. Over-depletion of the substrate reduces lateral diffusion since the charge transport velocity increases with large electric fields. Recent design changes have produced devices that can operate at substrate voltages exceeding 200 V [3].

The LBNL CCDs are well-suited for space and ground-based astronomical imaging and spectroscopy. The devices tested here were developed specifically for a large pixel-count focal plane in the proposed Supernova/Acceleration Probe (SNAP) [4], a satellite experiment designed to observe approximately 2000 high-redshift supernovae and carry out a weak-lensing survey to study dark energy. For good quantum efficiency in the near-infrared, the SNAP CCDs will have a substrate thickness of 200 μm, while for optimal spatial resolution for weak lensing the rms PSF is required to be 4 μm. We describe here the characterization of the lateral charge diffusion in these thick, high voltage CCDs as a function of the applied bias voltage using a previously reported technique [5].

II. Measurement Principle

The virtual knife edge method, originally developed in [5], is based on the Foucault knife edge technique, used to determine the profile of a light beam. An obstructing device is placed at the focus of a pinhole projector. The projected beam is scanned across the object edge. Data for intensity versus beam position, assuming a Gaussian beam profile, can be fitted to an error function and the beam width extracted.

The idea behind a virtual knife edge experiment is similar. Instead of a physical obstruction blocking the light, a region of pixels is used, the integration area, over which the signal from the spot is summed. A set of images is acquired as the spot is moved out of the integration area and the integrated intensity changes. The area edge serves the same function as

Manuscript received February 28, 2006. This work was supported by U.S. Department of Energy contract No. DE-AC03-76SF0098.

N. A. Roe is the corresponding author, with the Lawrence Berkeley National Laboratory, Berkeley, CA 94720 USA (telephone: 510-486-6380, e-mail: NARoe@lbl.gov).

J. A. Fairfield, D. E. Groom, S. J. Bailey, C. J. Bebek, S. E. Holland, A. Karcher, W. F. Kolbe, and N. A. Roe are with the Lawrence Berkeley National Laboratory, Berkeley, CA 94720 USA.

W. Lorenzon is with the University of Michigan, Ann Arbor, MI 48109 USA.

the physical knife edge experiment, hence a virtual knife edge. Fig. 1 is an illustration of the concept. This technique has the advantage of being independent of the physical pixel size and having no scattered light from a physical knife edge.

Plotting the total light in the integration area for each image scan position follows an error function with a transition width determined given by the convolution of the beam width and the CCD lateral diffusion. Fitting the scan data with an error function or its derivative with a Gaussian yields a measurement of the lateral charge diffusion.

III. Experimental Apparatus

The CCD is measured at 133 K inside a liquid-nitrogen cooled dewar operated at 10^{-7} torr. We use a Lakeshore autotuning temperature controller to control the temperature to within 0.1 K. The front of the dewar has an anti-reflection coated glass window and a shutter and faces into a light-tight box. An Oriel monochromator driven by a xenon arc lamp is used to provide light via an optical fiber to a 10 μm pinhole followed by a 25 mm long collimator. Scattered light is reduced by a blackened, threaded baffle on the inside of the tube. The collimated pinhole is focused on the CCD by a Mitutoyo 34 mm working-distance microscope objective. The theoretically achievable FWHM of the focused light beam is 2.6 μm at 550 nm. The projector sits inside the light-tight box on an *x*-*y*-*z* translation stage. The motor stage is carefully aligned so that the *x*-axis is parallel to the CCD rows and the *z*-axis is parallel to the columns. Both axes are coplanar with the CCD surface.

The CCD is controlled and read out by a modified Astronomical Research Cameras Gen II controller. The supplied utility board is configured to control the exposure timing, shutter operation, *x*-*y*-*z* motion of the projector, and position encoder readout. Java-based software manages the controller for data acquisition, and the data are analyzed using tools developed in Research Systems, Inc IDL.

IV. Experimental Procedure

A. Preliminary Measurements

The Foucault knife-edge technique was implemented with a razor blade. The rms beam size was measured to be 1.2 ± 0.1 μm, which is consistent with diffraction and the geometry of the setup. To focus the spot on the CCD, we start with an over-depletion substrate voltage of 55 V. We first center the spot on one pixel; then we adjust the distance from the projector to the CCD using the motorized focus stage and compare the signal in the nearest-neighbor pixels to the central pixel. When the ratio of the two is minimized, the spot is focused. We were able to obtain a focus precision of 20 μm. We could maintain focus for up to eight hours.

We used the ratio of nearest neighbors to the central pixel to test whether the focused spot remained on-axis after significant lateral translation by scanning multiple times in all directions and noting the drift. We found an average drift in the *x*-direction of 0.40 μm per 100 μm of motion in the *z*-direction, and 0.76 μm of drift along the *z*-axis per 100 μm of motion along the *x*-axis. In a normal scan, covering 200 μm along the *x*-axis, the drift was less than 0.5%, which is not significant.

Pixel-to-pixel non-uniformity can complicate the lateral diffusion measurements. Because of variations in the fabrication process, different pixels may have slightly different light response. To determine the degree to which this would affect our data, we scanned the spot across several pixels and then plotted the pixel response. We found that the pixel response was uniform to within 2% using a flat field, small enough that we deemed correction unnecessary.

B. Diffusion Measurement

Our scans varied in substrate voltage from 3 to 115 V and each had 150 images on average. The scans covered 10–60 pixels with step size from 0.4–40 μm. We varied the step size as a function of voltage since, at low voltages, diffusion is large and large step sizes more efficiently spanned the pixels containing the charge. The size of the integration area was also varied with substrate voltage. A square of about five times the rms diffusion on each side was used for the integration area; larger integration squares introduced additional read noise and degraded the fit error, while smaller integration squares did not completely contain the spot image. Fig. 2 shows the collected charge distribution in an array of CCD pixels at several voltages, demonstrating the variation of diffusion with voltage.

To optimize the signal-to-noise ratio, we adjusted the exposure time to have as many photons as possible without saturating the pixels. Exposure times varied from 0.1–10 seconds. At low voltages, longer exposure times were required since charge diffused into more neighboring pixels. At high voltages, we were careful to keep the exposure time short enough to avoid saturating the central pixel and blooming into neighboring pixels.

During data taking we monitored the baseline level of the CCD. We repeated measurements for any scan point that exhibited abnormal fluctuations due to excess background noise. We also scanned over the same set of pixels each time to avoid any potential pixel-to-pixel variation. All of the data were taken with 550 nm light and all the scans were taken across the channel stops (along the *x*-axis). Previous work showed no difference between diffusion measured in the row and column directions, and no difference between diffusion measured using different wavelengths of visible light [5].

Once the setup was completed and the spot size was characterized, we collected data with a device similar to the one previously characterized [5]. We reproduced the previous results. We then moved on to the high voltage SNAP CCD, a 3512×3512, 193 μm thick, 10.5 μm pixel, back-illuminated device. Fig. 3 shows a typical scan's data and its derivative. Also shown are fits to an error function and a Gaussian, respectively. The Gaussian-fit rms diffusion from the fit method as a function of substrate voltage is plotted in Fig. 4 and listed in Table 1.

C. Systematic and Statistical Errors

Once we had taken scans, we checked the robustness of the data in several ways. We compared error function and Gaussian fits to the data. The diffusion results were in good

agreement, but the Gaussian method was found to be less sensitive to fluctuations at the end points of the scan. We also collected data for several sizes of integration areas and several positions of the virtual knife edge in the software. Similar results were obtained within the statistical errors.

We investigated statistical uncertainties due to shot noise and read noise. The read noise was ~20 analog to digital units (ADUs), small compared to the shot noise on the signal, which varied from 300−750 ADUs (2-5%) for most substrate voltages. The measurement error was dominated by the statistical uncertainties on the data points due to shot noise; we took a large number of data points in order to mitigate this.

There can be systematic errors, discussed above, due to pixel-to-pixel non-uniformity and focus precision. The pixel-to-pixel uniformity error was found to be small. The focus drifted by small amounts, but not significantly during scans.

V. THEORY

We first review the original theory (initially developed in [6]), and then describe modifications required to fit the data accurately. The charges generated at the backside of a CCD and collected at the frontside gate structures are Gaussian distributed with distribution determined by the electric field shape, the diffusion coefficient and the transit time. If the CCD is not fully depleted, diffusion is dominated by the field-free region; the field is zero in the field-free region and increases linearly to $E_{\max}$, the electric field at the buried channel-substrate junction. If the CCD is fully depleted, the field increases linearly from E_D at the backside ohmic contact to $E_{\max}$. We consider these two cases separately.

A. Diffusion in an Over-depleted CCD

The charge drift velocity, v_d, is proportional to E at low E: $v_d = \mu E$ where μ is the carrier mobility. We can integrate this equation [6], to find the over-depleted diffusion variance

$$\sigma_{od}^2 = \frac{2k_BT}{q}\frac{\varepsilon_{Si}}{qN_D}\ln\left(\frac{E_{max}}{E_{min}}\right), \qquad (1)$$

where we have used the Einstein relationship $D/\mu = k_BT/q$. D is the diffusion coefficient, k_B is the Boltzmann constant, T is the temperature in Kelvin, q is the electron (or hole) charge, ε_{Si} is the permittivity of silicon, and N_D is the dopant density. For high constant fields, i.e., neglecting space charge in the depleted region, the asymptotic form of (1) [1], is

$$\sigma_{asymp}^2 = 2\frac{k_BT}{q}\frac{y_D^2}{V_{sub}-V_{J'}}, \qquad (2)$$

where y_D is the device thickness, V_{sub} is the substrate voltage, and $V_{J'}$ is the effective junction potential. For high substrate voltages, between 50–115 V, we can use the asymptotic form to predict the diffusion.

B. Diffusion in a CCD with a field-free region

In the case of a CCD that is not fully depleted, diffusion in the field-free region dominates. In this case, the total rms width is approximately equal to the thickness of the field-free region [7]. We can write this as the device thickness minus the thickness of the depleted region:

$$\sigma_{ff} = y_D - \sqrt{\frac{2\varepsilon_{Si}}{qN_D}(V_{sub}-V_{J'})}\,. \qquad (3)$$

In the region where the diffusion contributions from the field-free and depleted regions are comparable, we use an interpolation algorithm developed in [7] to predict the diffusion.

C. Comparing Data to Theory

In order to compare our data to theory, we first used equation (3) to fit the quantity $(y_D - \sigma_{ff})^2$, which is linear at low voltages. We extracted a depletion voltage of 18.1 V, a dopant density $N_D = 1.2\times10^{12}$ cm^{-3}, and a junction voltage $V_{J'}$ = −17.1V. The fit is shown in Fig. 5. With these parameters we calculate the diffusion given by (1). At voltages well above the depletion voltage, our data were consistently 30–40% above the theoretical predictions. After repeated checks of the apparatus, beam size, and fit calculations, we remained convinced of the accuracy of our experimental data.

D. New Developments in the Theory

We believe the discrepancy between the data and the asymptotic theory lies in the degradation of carrier mobility with increasing electric field. At low electric fields, charge velocity and charge transit time depend linearly on field strength. As field strength increases, the velocity field-dependence becomes non-linear as the scattering of energetic charge carriers increases, primarily due to optical phonon emission [8]. This effect can be expressed as a correction to the carrier mobility [9]. The mobility is modified such that

$$\mu(T,E) = \frac{\mu_0(T)}{m(T,E)}, \qquad (4)$$

where $\mu_0(T) = 1.31\times10^8 T^{-2.20}$ cm^2/V−s is the low-field mobility and $m(T,E)$ is a correction factor given by

$$m(T,E) \approx \left[1+\left(E/E_c\right)^{\beta}\right]^{1/\beta}, \qquad (5)$$

where the critical field $E_c = 1.24T^{1.68}$ V/cm and $\beta = 0.46T^{0.17}$ [10]. The drift velocity can now be written using the modified mobility

$$v_d(T,E) = \mu(T,E)E\,. \qquad (6)$$

For high fields, we can replace E by its average value $\langle E\rangle$ and calculate the transit time, t_{tr}, for a device of thickness y_D:

$$t_{tr} = \frac{y_D}{v_d} = \frac{y_D}{\mu(T,E)E} \qquad (7)$$

$$= \frac{{y_D}^2}{\mu(T,E)(V_{sub} - V_J)}. \quad (8)$$

Using this high-field transit time to find the asymptotic diffusion yields

$$\sigma^2_{asymp} = 2Dt_{tr} = 2\frac{D}{\mu(T,\langle E\rangle)}\frac{{y_D}^2}{(V_{sub} - V_J)}, \quad (9)$$

where D is the diffusion coefficient. Using Einstein's equation again, the resulting expression for the asymptotic lateral charge diffusion is

$$\sigma^2_{asymp} = 2\frac{k_B T}{q}\frac{y_D^2}{(V_{sub} - V_J)} m(T,\langle E\rangle). \quad (10)$$

This asymptotic form better fits the data at voltages significantly above the depletion voltage. There is still a small disparity near the depletion voltage, where the data are higher than the improved theoretical predictions. It is possible that there are additional temperature and field dependences in the diffusion coefficient [11]. Overall, the inclusion of the field dependence of mobility yields excellent agreement between data and theory at high voltage. The revised theoretical predictions are plotted in Fig. 4.

VI. Conclusions

We created a stable experimental setup for measuring charge diffusion in CCDs. We measured lateral charge diffusion in thick, fully-depleted CCDs. The voltage dependence of the experimental data motivated a modification of the theory to correctly account for velocity saturation effects. Our measurement, at a substrate voltage of 115 V is 3.71 ± 0.16 μm rms and meets the SNAP requirements. Future work will include intrapixel response studies, measurements of effects at the edge pixels of the CCD and investigation of near infrared lateral charge diffusion.

References

[1] S. Holland et al., "Fully-Depleted, Back-Illuminated Charge-Coupled Devices Fabricated on High-Resistivity Silicon", IEEE Trans. Electron Dev. Vol. 50 (3), 2003.

[2] C. J. Bebek et al., "Proton radiation damage in p-channel CCDs fabricated on high-resistivity silicon", IEEE Trans. Nucl. Sci., Vol. 49, pp. 1221–1225, 2002.

[3] W. F. Kolbe, S. E. Holland, and C. J. Bebek, "CCD development progress at Lawrence Berkeley National Laboratory", Proc. Scientific Detector Workshop 2005, submitted to proceedings of the Scientific Detector Workshop 2005, Taormina, Italy.

[4] G. Aldering et al., "Overview of the Supernova/Acceleration Probe (SNAP)", Proc. SPIE Vol. 4835, pp. 146–157, 2002.

[5] A. Karcher et al., "Measurement of Lateral Charge Diffusion in Thick, Fully Depleted, Back-illuminated CCDs," IEEE Trans. Nucl. Sci. Vol. 51 (5), pp. 2231–2237, 2004.

[6] S. E. Holland et al., "Development of back-illuminated, fully-depleted CCD image sensors for use in astronomy and astrophysics," Proc. IEEE Workshop on Charge-Coupled Devices and Advanced Image Sensors, Bruges, Belgium, pp. R26-1–R26-4, 1997.

[7] D. Groom et al., "Point-spread function in depleted and partially depleted CCDs", Proc. 4th ESO Workshop on Optical Detectors for Astronomy, pp. 205–216, 1999.

[8] S. M. Sze, "Physics of Semiconductor Devices," Chapter 1, John Wiley and Sons, 1981C.

[9] C. Jacoboni et al., "A Review of Some Charge Transport Properties of Silicon", Solid State Electronics Vol. 20, pp. 77–89, 1977.

[10] C. Canali et al., "Electron and Hole Drift Velocity Measurements in Silicon and Their Empirical Relation to Electric Field and Temperature", IEEE Trans. Electron Dev. Vol. 22, pp.1045–1046, 1975.

[11] D. J. Bartelink and G. Persky, "Diffusion of electrons in silicon transverse to a high electric field," Appl. Phys. Lett., 16 (5), pp. 191–194, 1970.

[12] L. Reggiani, R. Brunetti, and E. Normantas, "Diffusion coefficient of holes in silicon by Monte Carlo simulation," J. Appl. Phys., 59, (4), pp. 1212–1215, 1986.

[13] J. M. Hinckley and J. Singh, "Anisotropic high-field diffusion of holes in silicon," Appl. Phys. Lett., 66 (20), pp. 2727–2729, 1995.

Figures

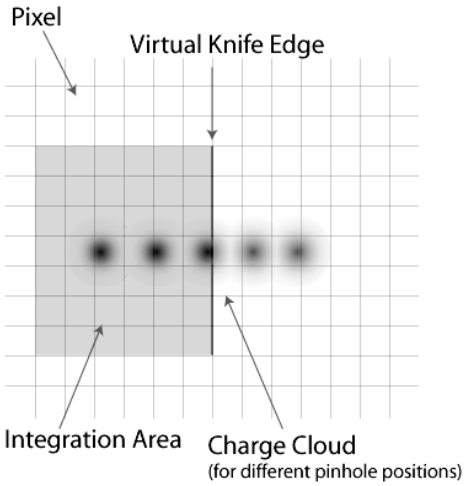

Fig. 1. The virtual knife edge concept. The spot is scanned to the right over the pixels on the CCD and eventually exits the integration area. The summed charge in the area square exhibits an error function shape.

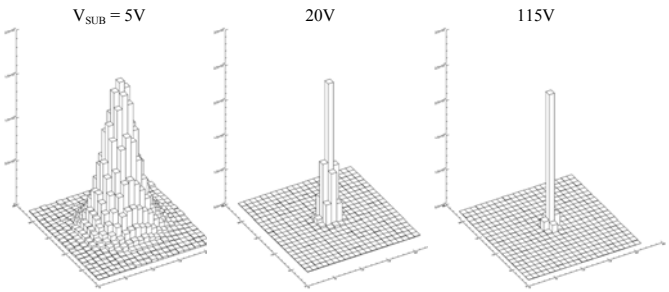

Fig. 2. The CCD response profile to a 1.2 μm rms beam spot for three different substrate bias voltages. Full depletion is reached at 20 V. Each grid box is a 10.5 μm pixel and the height is the detected charge.

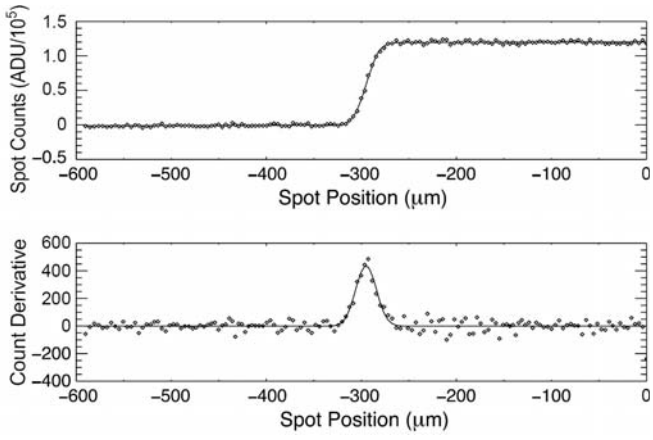

Fig. 3. Sample scan analysis. The top plot is the measured CCD counts in the integration area versus the beam position; the bottom plot is the derivative of the top. The top data can be fit with an error function, and the bottom data can be fit with a Gaussian. Both fits are obtained and compared as a consistency check. For these data, the error function sigma is 10.8 ± 0.002 μm, and the Gaussian sigma is 10.9 ± 0.6 μm

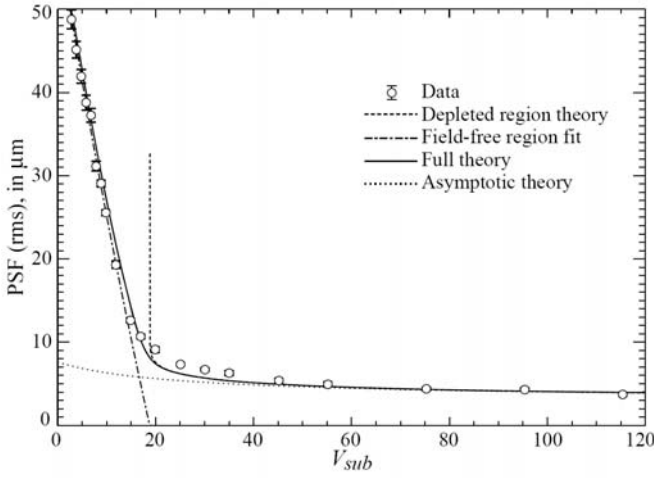

Fig. 4. The measured rms diffusion (data points) as a function of the substrate bias voltage. The data are for a 193 μm thick high voltage CCD, and at the highest voltage, the diffusion is lower than the 4 μm SNAP design goal. The field-free region line is the theoretical fit for operation below full depletion, the depleted region line is the theoretical prediction for over-depleted operation, and the full theory line is the convolution of both.

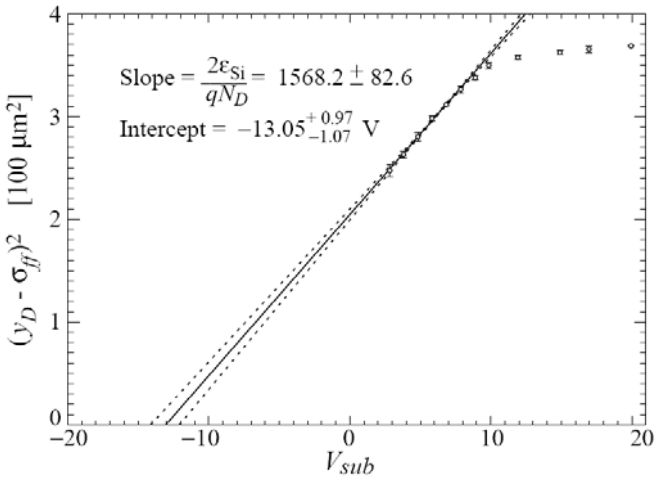

Fig. 5. The low-voltage linear fit used to determine parameters for the high-voltage fit. Here the square of the wafer thickness minus diffusion is plotted against the substrate voltage. The V_{sub} intercept is the junction voltage and the slope contains the carrier density.

TABLE I
RMS DIFFUSION MEASUREMENTS VERSUS SUBSTRATE BIAS VOLTAGE.

V_{sub} (V)	Diffusion (μm)	Error (μm)
2.84	48.8	1.1
3.82	45.1	1.0
4.83	41.9	0.9
5.83	38.8	0.9
6.84	37.3	0.8
7.87	31.1	0.6
8.89	29.1	0.4
9.86	25.6	0.4
11.91	19.3	0.4
14.90	12.6	0.3
16.96	10.7	0.3
19.94	9.1	0.3
25.10	7.3	0.2
30.10	6.7	0.2
35.04	6.3	0.3
45.20	5.4	0.3
55.20	4.9	0.3
75.30	4.4	0.2
95.40	4.3	0.2
115.40	3.7	0.2

The beam spot size has been subtracted in quadrature. The errors are statistical only.